Strain localization in Ti and Ti-alloys using three-dimensional topographic imaging

Ali Rouwane, Damien Texier, Samuel Hémery, Jean-Charles Passieux, Quentin Sirvin, J. Genée, Arnaud Proietti, Jean Charles Stinville

STRAIN LOCALIZATION IN Ti AND Ti-ALLOYS USING THREE-DIMENSIONAL TOPOGRAPHIC IMAGING

Ali Rouwane[1], Damien Texier[1], Samuel Hémery[2], Jean-Charles Passieux[1], Quentin Sirvin[1], Julien Genée[1], Arnaud Proietti[3], Jean-Charles Stinville[4]

[1] *Institut Clément Ader (ICA) – UMR CNRS 5312 ; Université de Toulouse ; CNRS, IMT Mines Albi, INSA, ISAE-SUPAERO, UPS ; Albi, France.*
[2] *Institut Pprime - UPR CNRS 3346 - ISAE-ENSMA ; Futuroscope-Chasseneuil Cedex, France.*
[3] *UAR Raimond Castaing, Université de Toulouse, CNRS, INP, UPS, INSA ; Toulouse, France.*
[4] *University of Illinois at Urbana-Champaign ; Urbana, USA*

High-resolution imaging over large fields of view was used to evidence nanometer-scale elementary and irreversible deformation mechanisms in a Ti6242S alloy with a lamellar microstructure. Intense strain localization was observed in specific colonies and former β-grains. High Resolution-Digital Image Correlation (HR-DIC) under a laser scanning confocal microscope (LSCM) was used to assess quantitative in-plane strain fields from the macroscopic to the microscopic scales at different tensile loading levels. A new stitching algorithm was developed in order to correct lens distortion with a self-calibration method using a global formulation that minimizes the gray-level disparity on overlapped regions of consecutive images in a mosaic. This correction aimed to better identify slip activity at the sub-grain level/lamella level. Topographic information from LSCM height maps successfully depicted out-of-plane strain localization at the lamella scale. The tested material presented large former β-grains with specific crystallographic orientations inherited from processing, leading to heterogeneous deformations at the mesoscopic scale.

Keywords: Commercial pure titanium; oxygen embrittlement; micromechanical tensile testing; image stitching; distortion; gradient of properties; mechanical behavior.

1. Introduction

Forging routes of titanium and titanium alloys in the β and α/β temperature range can lead to strong local texture in the form of macrozones for equiaxed or duplex microstructures [1,2], which are also denoted as "microtextured regions" (MTR) in the literature, or "feather-like structures" for lamellar microstructures [3,4]. The presence of these microtextured regions leads to heterogeneous strain distributions at the mesoscale and can significantly impair the fatigue life of these structural materials under fatigue and dwell-fatigue loadings [4–11]. Understanding strain localization in titanium and titanium alloys is central to better depicting how individual grains/lamellae/colonies plastically deform and how the crystallographic orientation distribution, *e.g.*, the local texture, affects the strain distribution within large regions of interest [12]. High-resolution imaging over large fields of view is vital in detecting the nanometer-scale elementary and irreversible deformation mechanisms as a function of the variability of mesoscopic deformation inherited from the former millimeter-scale β-grains [4,7,9]. Automation of imaging acquisition systems for either scanning electron microscopy [13,14] or optical microscopy [4,9,11,15] enables mosaic of images for large regions of interest with a spatial resolution compatible with the assessment of sub-grain strain localization when paired with high Resolution-Digital Image Correlation (HR-DIC). While HR-DIC is increasingly used to the quantitative evaluation of strain distribution, this technique requires the acquisition and registration of reference images compared to deformed images that conventional slip trace analysis techniques do not need. Depending on the in-plane and out-of-plane nature of the slip system, slip traces can be observed on micrographs and/or height maps, showing the complementarity of these characterization [15]. Therefore, the present study focuses on using laser scanning confocal microscopy (LSCM) to characterize slip activity at the sub-grain level on a large region using a fully automated image acquisition for reflective intensity maps and height maps. Topographic analyses and digital image correlation techniques will document the out-of-plane and in-plane response of the material subjected to tensile loading, respectively. Our motivation is to identify slip activity within different microtextured regions in relation to their crystallographic orientation.

2. Material and experiments

2.1. Material

The studied material is a near α Ti-6242S alloy (forged in the β-domain) with a chemical composition reported in **Table 1**. Inductively Coupled Plasma Optical Emission Spectroscopy (ICP-OES) was used to quantify major metallic elements, Glow Discharge Mass Spectrometry (GDMS) for metallic impurities, and Instrumental Gas Analysis (IGA) for gaseous species.

Table 1: Chemical composition of the Ti6242S material (in wt. %)

Ti	Al	Sn	Zr	Mo	Si	Fe	O
Bal	5.8	2.0	4.3	1.9	0.1	0.02	0.12

The material exhibits a Widmanstätten microstructure with α lamellae thickness about 2-3 µm. The microstructure at different scales is depicted in **Figure 1**. Based on the arrangement of the colonies, the present material presents millimeter-size former β-

grains. For more details on the microstructure, please refer to Ref. [16].

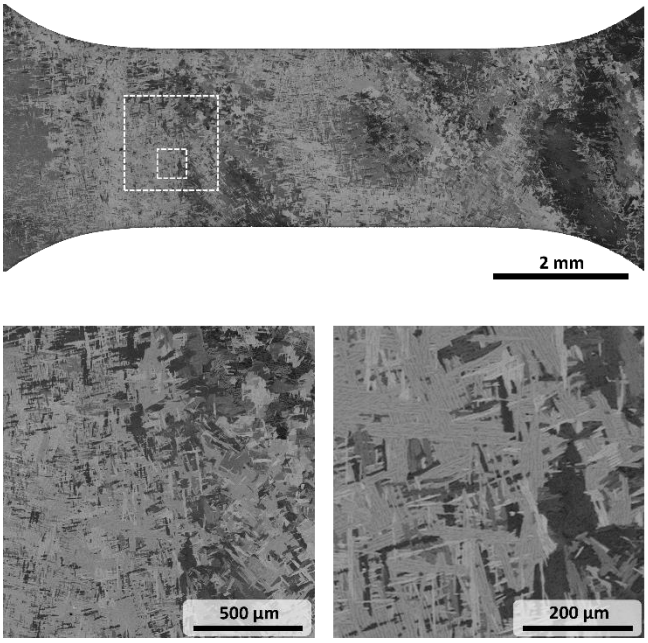

Figure 1: Microstructure of the Ti6242S alloy at different scales

2.2. Microtensile specimen preparation and characterization

Microtensile specimens were machined using electro-discharge machining. They were polished down to a 1 µm diamond finishing, then a mechanochemical polishing using colloidal silica with 70 % vol. hydrogen peroxide was carried out. A vibratory polishing is performed with the BUEHLER VibroMet 2 polisher for 3 h. This surface preparation technique is needed for electron backscattered diffraction (EBSD) analyses before deformation. EBSD maps were performed using a JEOL JSM 7100F scanning electron microscope with a CMOS Symmetry S2 EBSD detector (Oxford Instruments). A mosaic of EBSD maps was acquired at a magnification of x1000 with a step size of 1 µm with an observation area of 5.2 × 2.7 mm² (384 individual fields).

2.3. Interrupted tensile testing

Interrupted tensile tests were conducted at room temperature on an Instron 5800R electromechanical tensile testing machine with a load-cell of 5 kN. Tensile tests were carried out using a constant crosshead displacement rate for an equivalent strain rate in the plastic regime of 10^{-3} s^{-1}. Tensile tests were interrupted at five stress levels: 879, 918, 949, 997, and 1026 MPa. For information, the 0.2 pct. Yield strength of the material was 970 MPa at a similar strain rate.

2.4. Image acquisition for high resolution-digital image correlation (HR-DIC)

High resolution-digital image correlation (HR-DIC) technique was used in order to assess the kinematic fields at the specimen surface after deformation. This technique aims at tracking features on micrographs taken before and after deformation. Tracking several regions on a micrograph allows measuring displacement fields with a precision compatible with the slip activity at the sub-grain level, depending on the image acquisition technology. In the present study, an OLS5100LEXT (Olympus®) laser scanning confocal microscope (LSCM) was used for image acquisition. Both height and reflective laser intensity images were simultaneously recorded. Topographic images inform on the out-of-plane response of the material, while reflective laser intensity micrographs inform on the in-plane response. To cover the whole gage region, a mosaic of 25×10 images was automatedly acquired at x50 magnification (MPLAPON50XLEXT lens) with a resolution of 1024×1024 pixels², a size of 256 µm × 256 µm, and an overlap of 20% between consecutive micrographs. Each image was individually saved in order to further stitch the images. Images were acquired before deformation for reference, then after each interrupted tensile loading. The displacement fields were calculated at each stage by comparison between the initial image and the various successive images.

2.5. Speckle pattern preparation for high resolution-digital image correlation (HR-DIC)

The gold remodeling technique was used to obtain a speckle pattern compatible with the physical and numerical resolution of the micrographs. It consisted of a deposition of a thin and continuous film of gold (60 nm), then an exposure at 700 °C for 5 minutes, as depicted on the LSCM micrographs in Figure 4.

2.6. Lens distortion correction for high resolution-digital image correlation (HR-DIC)

As aforementioned, laser scanning confocal microscopy (LSCM) allows acquiring a high-resolution multi-view image of our sample. When performing classical image stitching, homographic transformations are usually searched by image registration; then, image warping is performed in order to average the image grey-level value on the overlapping regions [17]. LSCM is an optical observation apparatus and individual micrographs are generally distorted due to the light path going through a succession of lenses, mirrors, and light splitters. In the case of multi-view microscope image

stitching, this approach induces severe limitations as it does not dissociate the distortion transformation and the simple translation related to the physical multi-view acquisition. As a result, the overlapping regions in the final stitched images are blurred, which leads to inaccurate strain measurements when using DIC (see Figure 2, "without correction").

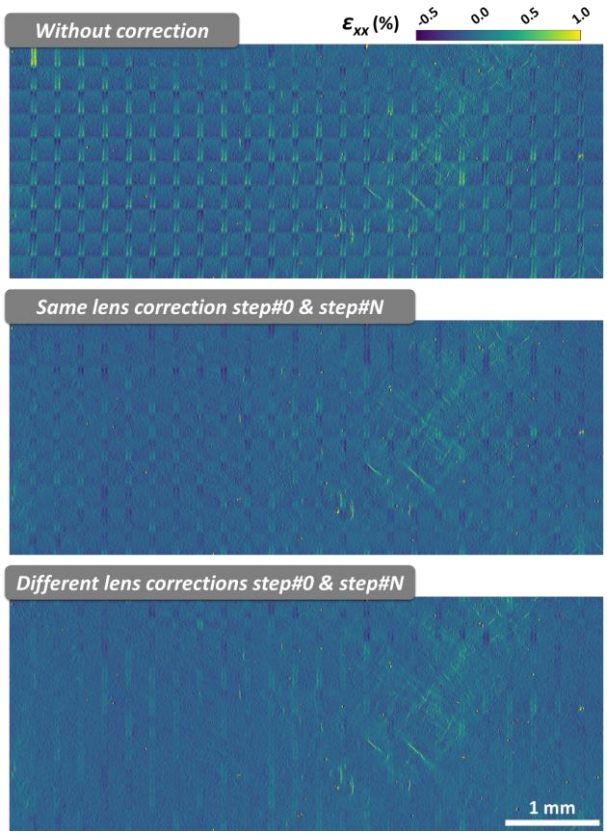

Figure 2: Influence of the lens distortion correction of the strain map of the whole region of interest at the onset of microplasticity: No correction, correction using the distortion function from the reference images, correction using the distortion function for each loading step.

In our case, the lens is fixed (except in the z-position) and the sample is automatedly moved via a motorized X-Y stage. Therefore, we can first consider that the lens distortion of our system is intrinsic to our light path, *i.e.*, from the lens to the Airy sensor, regardless of the image position. A global approach was formulated to identify at the same time the X-Y translation between the different images and the unknown intrinsic distortion related to the acquisition system. We consider solving a non-linear least squares problem whose unknowns are the non-periodic modes of the distortion function and the translations of consecutive images via overlapped regions. This self-calibration method is only based on the sample speckle pattern and may be seen as a bundle adjustment approach. To identify the distortion field, one may choose a distortion model. In our case, a simple two-dimensional cubic polynomial model is considered as the classical parametric lens models (such as the Brown-Conrady model [18]) were too restrictive for the considered LSCM microscopic lenses. The result of the distortion field is illustrated in Figure 3. The considered algorithm minimizes the gray level gap between the overlapped regions, improving the stitching quality. This allows for obtaining less noisy strain maps when using DIC (see Figure 2, "same lens correction"). Since the method is self-calibrated, it is possible to distort micrographs with distortion functions identified for each step since the lens distortion can slightly change. It is worth mentioning that the DIC calculation allows displacement measurement with sub-pixel accuracy, thus leading to very high sensitivity to the lens distortion calibration. The displacement and strain fields were calculated using the OpenCV library [19] running under Python. Lens distortion correction was found to greatly reduce noise in the overlapped regions compared to initial and conventional stitching techniques. This correction aimed to better depict microplasticity in some regions of the specimen gage. Therefore, images were all corrected using the lens distortion function identified at each acquisition sequence, *i.e.*, at each loading step. Interestingly, distortion displacements are between of ± 2 pixels for 1024×1024 pixel images.

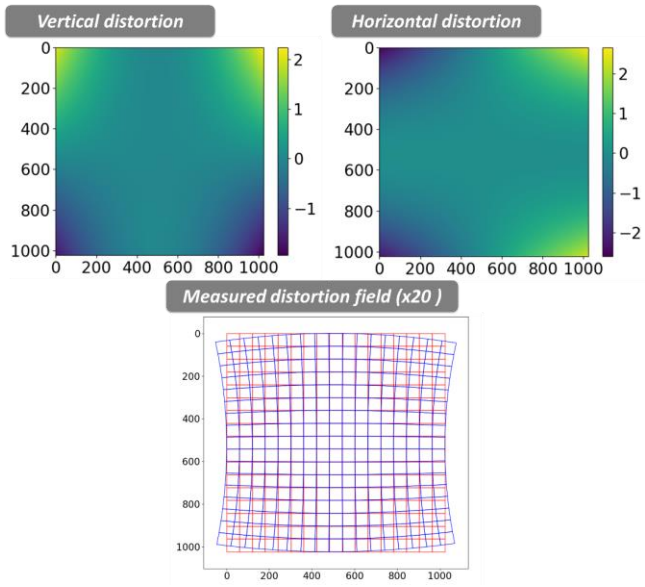

Figure 3: Evaluation of the lens distortion using digital image correlation on the overlap regions of the image mosaic. Vertical and horizontal distortion functions, illustration of the magnified measured distortion field (x20)

2.7. Slip trace analysis from height maps

Laser scanning confocal microscopy (LSCM) aims at measuring the height of a region of interest in a full-field manner. Due to speckle pattern application, surface irregularities were observed on initial

topographic images, *i.e.*, prior to deformation. Therefore, filtering techniques based on directional and morphological filters were used to dissociate and remove high-frequency noise from the speckle pattern to assess slip height steps due to slip activity at the free surface. An edge detection filter was then applied to document the out-of-plane displacement resulting from slip activity and early damage at the microstructure scale (see Figure 4). This technique is particularly effective since it does not rely on image comparison/correlation, and thus does not require images from the non-deformed specimen.

3. Results and discussion

3.1. Strain localization in an individual zone

The motivation of the present paper is to document the occurrence of early slip events at the microstructure scale. In a first attempt, the region of interest was limited to a single micrograph. The region of interest was constituted of a large colony (purple on the EBSD map in Figure 4). Optical and LSC micrographs evidenced the intricate lamellar microstructure. Height maps collected after loading at 997 MPa and 1026 MPa highlight height steps relative to local slip activity. Height variation using an edge detection function aimed at better depicting height steps from these discontinuities. The strain localization path is relatively wavy due to the interplay between intralamellar deformation slip transmission from lamella to lamella. Slip localization nearby α/β interfaces is also observed. Heigh steps and the frequency of slip events increased with the load application. Interestingly, strain localization develops through colonies with occasional bifurcations nearby α/β interfaces, as reported by Kloenne *et al.* [20]. Interestingly, the intensity of the height variation is not constant along slip events, the intensity being maximal in the core of the colony and minimal in the vicinity of other colonies due to deformation incompatibility. In addition, isolated slip events with an identical slip trace exhibited comparable intensity variation in both in-plane strain maps and height variation maps. In-plane strain maps are noisier than height variation maps to detect slip events. Consistency between the in-plane and out-of-plane techniques supports the application of height map variation for slip trace analyses. A correlation with EBSD analyses will aim to further demonstrate the capability to identify active slip planes in such tortuous strain localization paths. In addition, the LSCM provides a three-dimensional description of the kinematics field and, thus a three-dimensional description of the displacement jump for each plastic event. This analysis will be conducted to identify active slip systems in such a complex microstructure.

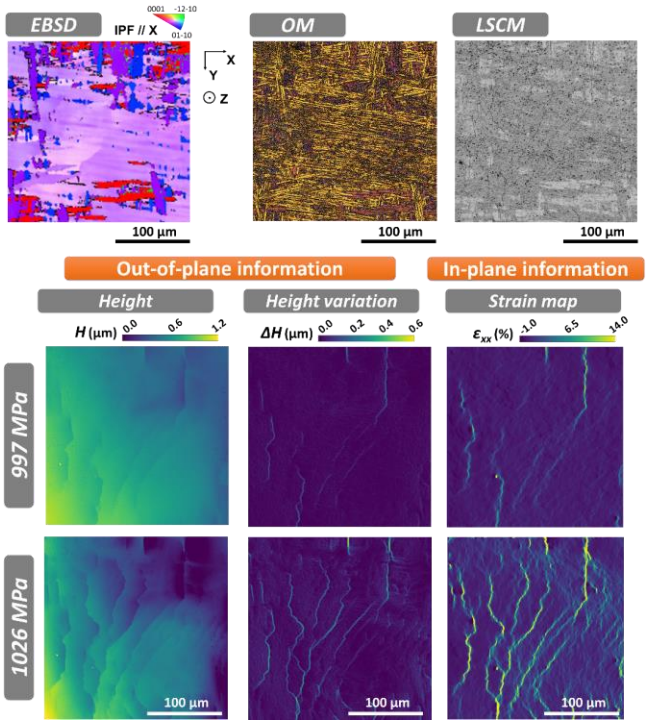

Figure 4: Evaluation of the in-plane and out-of-plane strain localization using HR-DIC with a LSCM on a single micrograph. Inverse pole figure map of the region of interest in reference to the loading direction, optical and laser scanning confocal micrographs, out-of-plane strain localization (height maps, height variation maps) and in-plane strain localization (strain maps) for applied stresses of 997 and 1026 MPa.

3.2. Strain localization to the whole gage region

After the demonstration of the microplasticity detection on a small region of interest, the technique was applied to the whole gage region of the microtensile specimen. As shown in Figure 1, the material presents a lamellar microstructure with colonies with sizes of tens to hundreds of micrometers (Figure 5). Crystallographic orientations of neighboring colonies gathered in former β-grains are governed by Burgers orientation relationship. Some large hard oriented regions, where the alignment of the [0001] direction with the loading direction leads to a difficult slip activity, are identified on the EBSD maps (red regions in Figure 5).

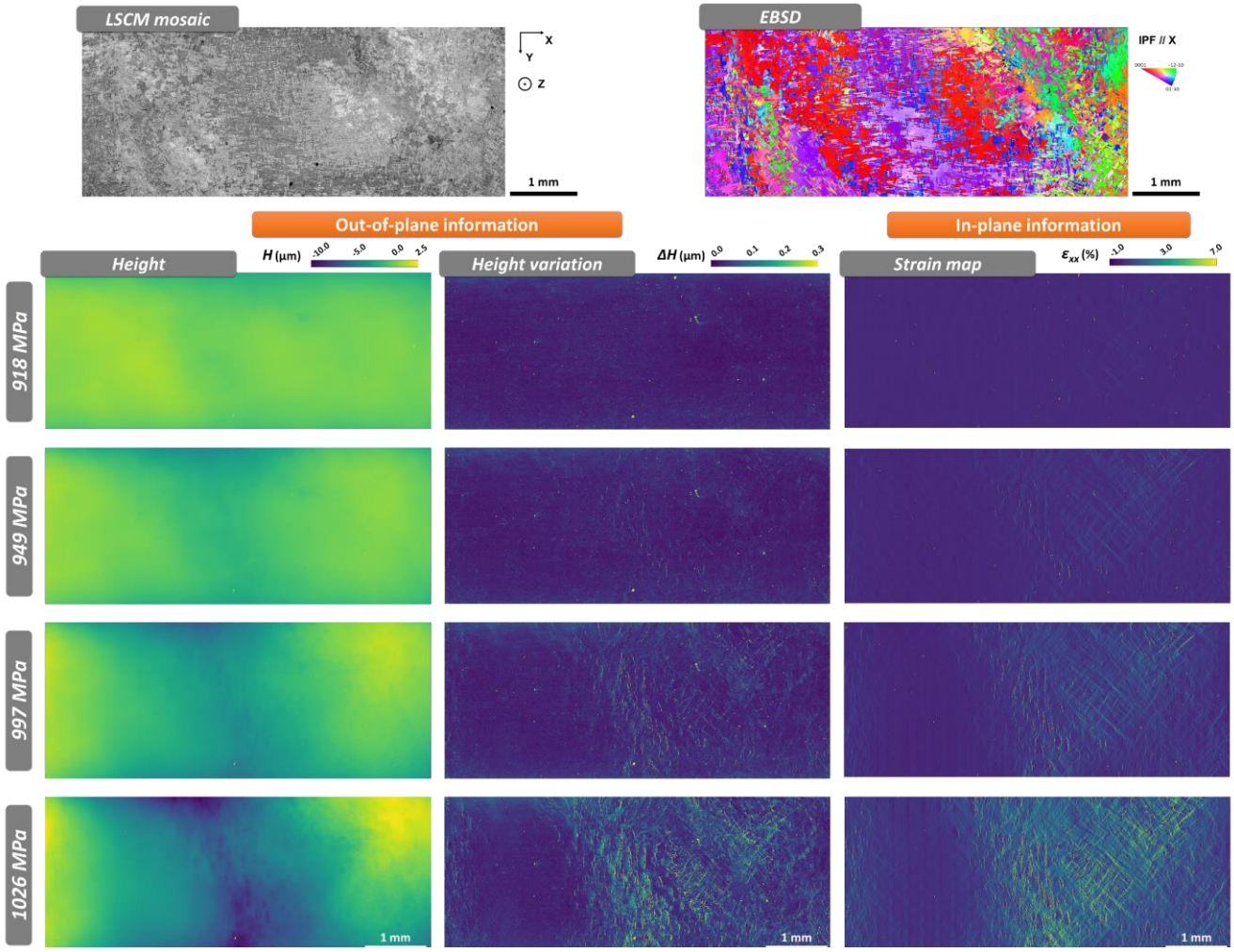

Figure 5: Evaluation of the in-plane and out-of-plane strain localization using HR-DIC with a LSCM on the whole region of interest. Laser scanning confocal stitched image composed of the 250 individual images, inverse pole figure map of the region of interest in reference to the loading direction, out-of-plane strain localization (height maps, height variation maps) and in-plane strain localization (strain maps) for applied stresses of 918, 949, 997 and 1026 MPa.

Both height variation and in-plane deformation maps evidence the heterogeneous distribution of slip events in relation to the local microstructure. Interestingly, the very first slip events appear at applied stresses between 879 and 918 MPa, at a stress below the macroscopic yield strength (Y.S. = 970 MPa). These microplasticity events are both observed on the height variation map and the in-plane strain map at 918 MPa. Plastic deformation was found to first occur in the central region of the sample, corresponding to the purple colour region on the EBSD maps in relation to the macroscopic loading direction. As for the individual region, different features including frequent slip transmission across retained β layers as well as slip localization along or nearby α/β interfaces developed within colonies. The relationship between the crystallographic orientation of colonies and the occurrence of microplasticity will be further developed. These results are in good agreement with the similar work of Lunt *et al.* [9], Huet *et al.* [4], and Yvinec *et al.* [11] on strain distribution evaluation at the mesoscale in relation to the intricate microstructure resulting from processing history of Ti alloys. In addition, minor differences in the detection of slip events were observed considering height variation maps and in-plane deformation maps, showing the complementary use and necessity of out-of-plane and in-plane information to accurately characterize such complex strain localization paths.

4. Conclusions

Strain localization was investigated at the microscale using both in-plane strain maps with Digital Image Correlation (DIC) techniques and height variation maps with laser scanning confocal microscopy. These techniques were applied on a complex lamellar microstructure, leading to complex and wavy slip

morphology within colonies due to gliding from lamella to lamella. These techniques were found complementary and aimed at identifying microplasticity at the intra-colony scale for a field of view containing several former millimeter-size β-grains. HR-DIC and topographic measurements using LSCM allow us to observe the three-dimensional character of slip activity using in-plane displacement as well as steps resulting from dislocations emerging at the free surface of the specimen. Interestingly, the height variation analysis does not require a reference image before deformation compared to HR-DIC, making the technique particularly effective for specimens with flat surfaces and initial low roughness deprived of the speckle pattern.

5. Acknowledgements

This research was funded, in whole or in part, by The European Research Council, project HT-S_4DefOx - Grant number 948007]. This research was funded, in whole or in part, by The International Research Project (IRP) CIN&MAT funded by the French National Center for Scientific Research (CNRS) – INSIS Institute. A CC-BY public copyright license has been applied by the authors to the present document and will be applied to all subsequent versions up to the Author Accepted Manuscript arising from this submission in accordance with the grant's open access conditions.

6. References

[1] L. Germain, N. Gey, M. Humbert, P. Bocher, M. Jahazi, Mater. Sci. Forum 495–497 (2005) 663–668.

[2] E. UTA, N. Gey, P. Bocher, M. Humbert, J. GILGERT, J. Microsc. 233 (2009) 451–459.

[3] D. Bhattacharyya, G.B. Viswanathan, H.L. Fraser, Acta Mater. 55 (2007) 6765–6778.

[4] A. Huet, A. Naït-Ali, T. Giroud, P. Villechaise, S. Hémery, Acta Mater. 240 (2022) 118348.

[5] F. Bridier, P. Villechaise, J. Mendez, Acta Mater. 56 (2008) 3951–3962.

[6] A.L. Pilchak, R.E.A. Williams, J.C. Williams, Metall. Mater. Trans. A Phys. Metall. Mater. Sci. 41 (2010) 106–124.

[7] M.P. Echlin, J.C. Stinville, V.M. Miller, W.C. Lenthe, T.M. Pollock, Acta Mater. 114 (2016) 164–175.

[8] D. Lunt, J.Q. da Fonseca, D. Rugg, M. Preuss, Mater. Sci. Eng. A 680 (2017) 444–453.

[9] D. Lunt, A. Ho, A. Davis, F. Martina, J. Hönnige, J. Quinta da Fonseca, P. Prangnell, in: 14th World Conf. Titan., 2020.

[10] Y. Liu, F.P.E. Dunne, Int. J. Fatigue 142 (2021) 105971.

[11] T. Yvinec, A. Naït-Ali, D. Mellier, D. Bertheau, J. Cormier, P. Villechaise, L. Rat, S. Hémery, Addit. Manuf. 55 (2022).

[12] S. Hémery, P. Villechaise, D. Banerjee, Metall. Mater. Trans. A Phys. Metall. Mater. Sci. 51 (2020) 4931–4969.

[13] J.C. Stinville, W.C. Lenthe, M.P. Echlin, P.G. Callahan, D. Texier, T.M. Pollock, Int. J. Fract. 208 (2017) 221–240.

[14] R.L. Black, T. Garbowski, C. Bean, A.L. Eberle, S. Nickell, D. Texier, V. Valle, J.C. Stinville, Exp. Mech. (2023).

[15] J.H. Liu, N. Vanderesse, J.C. Stinville, T.M. Pollock, P. Bocher, D. Texier, Acta Mater. 169 (2019) 260–274.

[16] K. Cave, D. Texier, E. Fessler, D. Monceau, D. Poquillon, Metall. Mater. Trans. A Phys. Metall. Mater. Sci. 54 (2023) 549–561.

[17] S. Preibisch, S. Saalfeld, P. Tomancak, Bioinformatics 25 (2009) 1463–1465.

[18] J. Weng, P. Cohen, M. Herniou, IEEE Trans. Pattern Anal. Mach. Intell. 14 (1992) 965–980.

[19] G. Bradski, Dr. Dobb's J. Softw. Tools (2000).

[20] Z. Kloenne, G. Viswanathan, S. Fox, M. Loretto, H.L. Fraser, Scr. Mater. 178 (2020) 418–421.